A Surface Energy Perspective on Climate Change

TIMOTHY ANDREWS AND PIERS M. FORSTER

School of Earth and Environment, University of Leeds, Leeds, United Kingdom

JONATHAN M. GREGORY

Walker Institute for Climate System Research, Department of Meteorology, University of Reading, Reading, and Met Office Hadley Centre, Exeter, United Kingdom

(Manuscript received 30 July 2008, in final form 13 November 2008)

ABSTRACT

A surface forcing response framework is developed that enables an understanding of time-dependent climate change from a surface energy perspective. The framework allows the separation of fast responses that are unassociated with global-mean surface air temperature change (ΔT), which is included in the forcing, and slow feedbacks that scale with ΔT. The framework is illustrated primarily using $2 \times CO_2$ climate model experiments and is robust across the models. For CO_2 increases, the positive downward radiative component of forcing is smaller at the surface than at the tropopause, and so a rapid reduction in the upward surface latent heat (LH) flux is induced to conserve the tropospheric heat budget; this reduces the precipitation rate. Analysis of the time-dependent surface energy balance over sea and land separately reveals that land areas rapidly regain energy balance, and significant land surface warming occurs before global sea temperatures respond. The $2 \times CO_2$ results are compared to a solar increase experiment and show that some fast responses are forcing dependent. In particular, a significant forcing from the fast hydrological response found in the CO_2 experiments is much smaller in the solar experiment. The different fast response explains why previous equilibrium studies found differences in the hydrological sensitivity between these two forcings. On longer time scales, as ΔT increases, the net surface longwave and LH fluxes provide positive and negative surface feedbacks, respectively, while the net surface shortwave and sensible heat fluxes change little. It is found that in contrast to their fast responses, the longer-term response of both surface energy fluxes and the global hydrological cycle are similar for the different forcing agents.

1. Introduction

Traditional energy imbalance arguments of the earth's climate system measure energy budget changes at the tropopause or top of atmosphere (TOA). Near-instantaneous changes to this energy balance caused by external factors are termed "radiative forcings," and have long been used to quantify the strength of many different climate change mechanisms (e.g., Houghton et al. 1990). The TOA radiative forcing concept has proven to be fundamental to understanding climate change because it gives a straightforward way of estimating global-mean surface air temperature change (ΔT) (e.g., Forster et al. 2007), which itself is related to regional changes, such as temperature and precipitation (e.g., Mitchell et al. 1999). In this paper we investigate what can be learned by applying a similar forcing and response concept to the earth's surface energy budget.

Despite early work, which highlighted the importance of the surface energy budget (e.g., Ramanathan 1981; Dickinson 1983), there is still a need to improve our understanding of it in the context of global climate change (e.g., National Research Council 2005). This is particularly so given that on the global scale the surface energy budget is closely related to the atmospheric heat budget and the earth's hydrological cycle (e.g., Mitchell 1983; Mitchell et al. 1987; Boer 1993; Allen and Ingram 2002). The global-mean response of the hydrological cycle is useful because it can be compared with recent global observations (e.g., Wentz et al. 2007) and the thermodynamic expectations of a constant relative humidity

Corresponding author address: Timothy Andrews, School of Earth and Environment, University of Leeds, Leeds, LS2 9JT, United Kingdom.
E-mail: t.andrews@see.leeds.ac.uk

DOI: 10.1175/2008JCLI2759.1

response. However, it may not in itself be that relevant for climate impacts, because regional changes to the hydrological cycle can be significantly larger than the global-mean change and of the opposite sign (e.g., Meehl et al. 2007).

The surface energy budget includes both radiative [longwave (LW) and shortwave (SW)] and nonradiative [sensible heat (SH) and latent heat (LH)] terms. Understanding links between radiative and nonradiative terms are important. For example, changes in the surface solar irradiance, resulting from the presence of reflecting and absorbing aerosols, may be balanced by changes in surface temperature and/or changes in the nonradiative fluxes (e.g., Ramanathan et al. 2001; Liepert et al. 2004; Wild et al. 2004). Increasingly, surface energy budget arguments are being used to describe climate forcings and climate change processes. Examples include the physiological forcing (e.g., Boucher et al. 2008), anthropogenic land cover change (e.g., Davin et al. 2007), land–sea warming contrast (e.g., Sutton et al. 2007), changes to cumulus convection (e.g., Pielke 2001), and forcing from irrigation (e.g., Boucher et al. 2004).

Many previous studies have only considered equilibrium conditions, that is, a difference between a perturbed steady state and the initial unperturbed state. Other recent studies concentrating on the TOA energy budget (e.g., Gregory and Webb 2008, hereafter GW08; Andrews and Forster 2008; Williams et al. 2008) showed that analysis of time-dependent changes can reveal fundamental information about the climate system that may have otherwise been missed by restricting analysis to the final steady state.

Here we follow an analogous path to GW08 by developing a forcing response framework that allows a time-dependent analysis of changes to the earth's energy budget in response to a climate forcing agent; here, the framework is developed for the surface, rather than the TOA. Such an analysis allows the budget to be split into the following two parts: surface forcing and climate response. As in Gregory et al. (2004) and GW08, the distinction between forcing and response is made on the basis of time scale, so that surface forcing measures the net surface heat flux caused by a climate forcing agent without time for any global climate response to have occurred, and the climate response refers to changes over longer time scales (i.e., years or decades when considering only the mixed layer of the ocean), defined here as changes to global-mean surface air temperature ΔT. Given the intimate relationship between the surface energy budget and the hydrological cycle, we will then show how this approach has practical value in revealing fundamental information about the response of the earth's hydrological cycle to climate forcings.

2. Surface forcing response framework

A TOA (denoted by a "prime") radiative flux imbalance N' is a combination of an imposed radiative flux F', resulting from a climate forcing agent, and a radiative response H', which responds on time scales of global temperature change. Usually H' is assumed to be proportional to ΔT, with a proportionality factor of α', where α' is often referred to as the climate feedback parameter. GW08 showed that the components (LW and SW) of N', F', and α', denoted by subscript i, all obey a simple linear relationship $N_i' = F_i' - \alpha_i' \Delta T$, so that the net TOA heating imbalance N' is equal to the sum of the N_i' components.

Now let us assume that the surface heat fluxes also obey a similar linear relationship. The results of GW08 (their Fig. 5) suggest that this is a reasonable assumption for the HadSM3 slab-ocean climate model forced by $2 \times CO_2$, and we will show that this is a robust feature across many slab-ocean climate models in section 3. The components of the surface energy budget, denoted by subscript j, are different than those at the TOA because they include the turbulent heat fluxes, LH, and SH. We assume these fluxes also respond to ΔT, with a surface feedback parameter α_j. Thus, for a given component of surface forcing F_j, we have $N_j = F_j - \alpha_j \Delta T$, where N_j is the surface energy imbalance. The net surface energy imbalance equation then reads

$$N = \Sigma_j N_j = \Sigma_j F_j - \Sigma_j \alpha_j \Delta T, \tag{1}$$

where j denotes the components of the net surface heat fluxes: LW, SW, LH, and SH.

To illustrate the application of this simple surface forcing response relationship, we consider the tropospheric heat budget. Our definition of forcing includes any adjustments to the stratosphere and troposphere that is unassociated with ΔT, that is, F is evaluated by N at the limit of $\Delta T \to 0$ (see GW08). This fully adjusted forcing must be the same throughout the troposphere (and the stratosphere for that matter), otherwise it would continue to store heat, which it cannot do for long because of its relatively small heat capacity. If the adjusted *radiative* forcing is not the same at the surface and the TOA, then there must be an induced turbulent component in the adjusted surface forcing to maintain the tropospheric heat balance. This means that climate forcing mechanisms may impact the earth's hydrological cycle before the time scale associated with global temperature change.

3. Results for a doubling of carbon dioxide

We test the validity and illustrate the use of the surface forcing response framework [Eq. (1)] using general

circulation model (GCM) experiments in which atmospheric CO_2 levels are instantaneously doubled ($2 \times CO_2$). The climate model data are based on the World Climate Research Programme's (WCRP's) Coupled Model Intercomparison Project phase 3 (CMIP3) multimodel dataset. This large database supports the Fourth Assessment Report (AR4) of the Intergovernmental Panel on Climate Change (IPCC), and contains the $2 \times CO_2$ experiment results, along with their corresponding control runs, for many of the world's leading GCMs. Note that we refer to the CMIP3 models by their official CMIP3 name, which usually refers to the GCMs coupled to a fully dynamical ocean, but we are using the corresponding models with slab oceans. We also make use of two different versions of the Met Office (UKMO) Hadley Centre Slab-Ocean Model, version 3 (HadSM3): one with and one without a sulfur cycle, HadSM3b and HadSM3, respectively (GW08 regarded the two as the same model for practical reasons, and here HadSM3b is the same as the "standard HadSM3" in GW08). In these two experiments CO_2 levels have been instantaneously quadrupled, but following GW08 we divide the results by two to apply this to $2 \times CO_2$.

a. Global climate change

Figure 1 shows the regression of changes in annual-mean global-mean surface heat fluxes N_j against annual-mean global-mean ΔT for the first 20 yr after CO_2 was doubled for various slab-ocean GCMs. All changes are determined as differences from the corresponding control run, and all fluxes are defined as positive downward. The time evolution begins on the left of the plots, where $\Delta T = 0$, and the surface forcing components F_j can be determined from y-axis intercepts. As time evolves ΔT increases and the surface heat fluxes respond according to $\alpha_j \Delta T$, where α_j is determined from the gradient of the regression lines. The new perturbed steady state, with an equilibrium temperature change ΔT_{2x} is reached when $N = 0$, that is, when the surface heating imbalance has been eliminated. All components for all models tend to follow straight lines and therefore support our linear analysis. It is a notable result that the simple linear surface forcing response framework governed by Eq. (1) is a robust feature across models. Furthermore, because the TOA energy budget also behaves in the same way (see GW08), we can infer that the tropospheric energy budget can be similarly separated into a forcing and response. It is the need to rebalance these energy budgets that drives climate change. We now proceed to examine how this is actually achieved.

Tables 1 and Tables 2 show the components of the diagnosed surface forcing F_j and the surface climate feedback parameter α_j, respectively. Hereafter, and in Table 2, we define $Y_j = -\alpha_j$ because this suits its physical interpretation better (GW08); that is, a positive Y_j represents a positive feedback on climate change. A comparison of the corresponding forcing components diagnosed from the TOA in GW08 with those diagnosed at the surface reveals that the *radiative* component of forcing is much smaller at the surface than at the TOA, ~ 0.9 W m^{-2} (Table 1), compared to the ~ 3.3 W m^{-2} (GW08) for the multimodel ensembles, respectively. CO_2 forcing is therefore predominantly absorbed by the troposphere, and thus directly reduces the tropospheric radiative cooling (e.g., Allen and Ingram 2002; Allan 2006; Lambert and Faull 2007). Although our forcing definition allows for adjustments that occur on time scales quicker than ΔT, this difference between surface and TOA CO_2 *radiative* forcing is predominantly an instantaneous effect (e.g., Collins et al. 2006) because the lower troposphere is thicker optically than the upper troposphere. Because the adjusted *radiative* forcing is greater at the TOA than the surface, the tropospheric heat budget must be maintained by a surface *turbulent* forcing component, found to be ~ 2.1 W m^{-2} for the multimodel ensemble (Table 1). This is predominantly composed of a surface LH forcing, $F_{LH} = 1.91 \pm 0.48$ W m^{-2}, which is similar across the models. This adjustment has consequences for the earth's hydrological cycle, and is discussed further in section 5. Comparing the net surface forcing (F_{Net}) with the TOA net forcing (F'_{Net}, determined by GW08; Table 1) we find that F_{Net} is slightly smaller than F'_{Net} in all models, implying that the atmosphere is continuing to store heat, but the reason and statistical significance for this remains unclear. We also note that Model for Interdisciplinary Research on Climate 3.2, medium-resolution version [MIROC3.2(medres)] is unusual in that it has a particularly small, if not negative, F_{LW} component and an overly large F_{SW} component compared to the other models.

The climate evolves with the feedback parameters Y_j, shown in Table 2. The LW component Y_{LW} is in good agreement across the models and is associated with a positive surface feedback on climate change because the atmosphere becomes warmer and moister as ΔT increases, and so the downwelling LW radiation at the surface also increases (e.g., Ramanathan 1981). Regressions of surface upwelling and downwelling LW radiation against ΔT reveals that LW up and LW down provide feedbacks across the models of ~ -5.2 W m^{-2} K^{-1} and ~ 6.2 W m^{-2} K^{-1} respectively, leading to $Y_{LW} \sim 1$ W m^{-2} K^{-1}, as in Table 2. The increase of LW down with ΔT therefore outweighs the thermal response of the earth's surface. This finding is consistent with Allan (2006) who analyzed reanalysis data and found

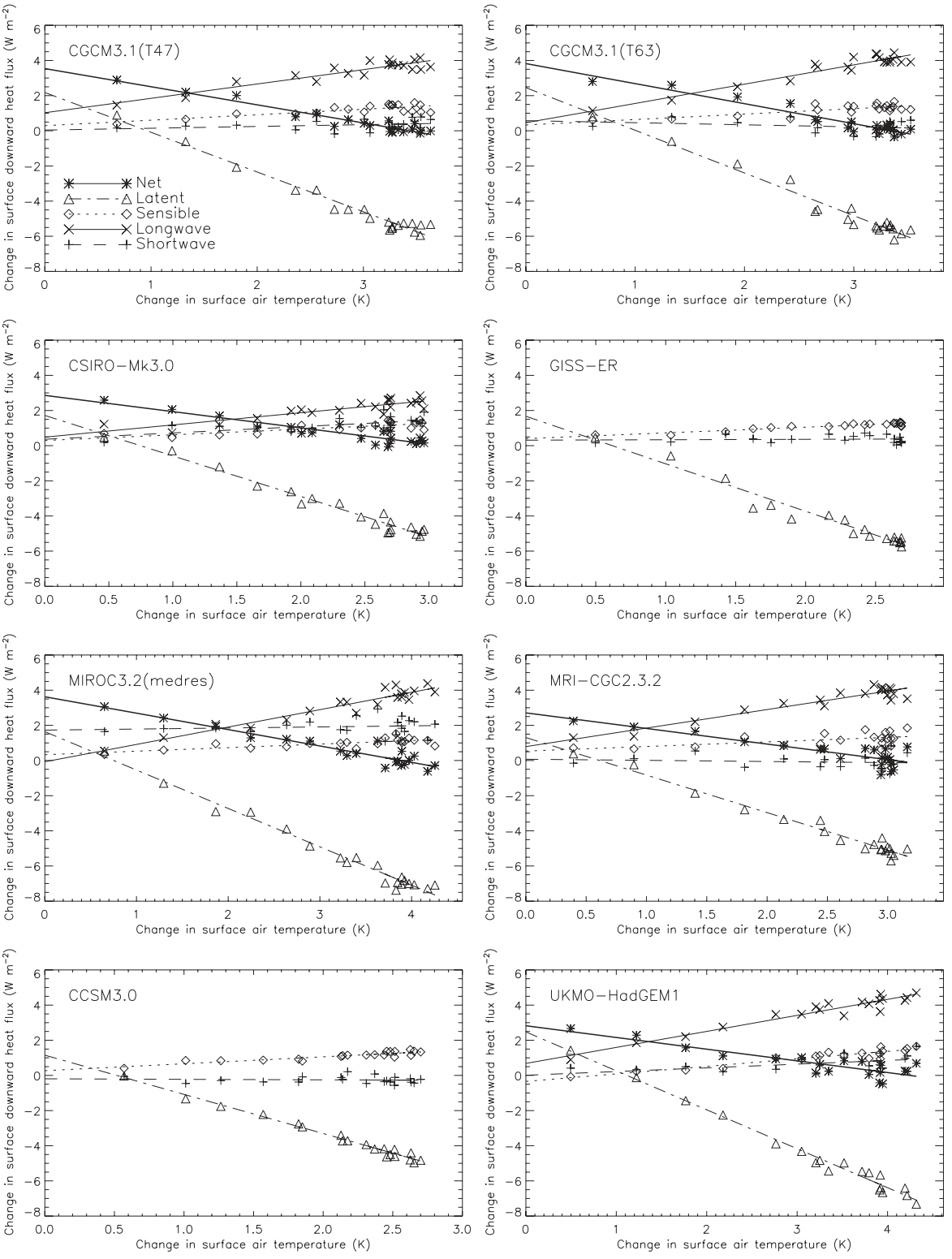

FIG. 1. Change in annual-mean global-mean surface heat fluxes N, as a function of annual-mean global-mean surface air temperature change ΔT for various slab-ocean GCMs forced by $2 \times CO_2$. All heat fluxes are defined as positive downward. The lines are the regressions and the symbols are annual means.

TABLE 1. Components of the global-mean $2 \times CO_2$ surface forcing (W m^{-2}) for various slab-ocean GCMs. Forcing components include fast responses that occur before ΔT, such as stratospheric and tropospheric adjustment. The uncertainty in the individual models and the model ensemble are ± 1 standard error from the regression and ± 1 standard deviation across the models, respectively. Also shown for comparison is the net TOA forcing (F'_{Net}) determined by GW08.

	F_{LW}	F_{SW}	F_{LH}	F_{SH}	F_{Net}	F'_{Net} (GW08)
Community Climate System Model, version 3.0 (CCSM3.0)	–	−0.19 ± 0.17	1.15 ± 0.14	0.27 ± 0.10	–	2.93 ± 0.23
CGCM3.1(T47)	1.03 ± 0.24	0.04 ± 0.24	2.18 ± 0.28	0.29 ± 0.17	3.54 ± 0.21	4.00 ± 0.35
CGCM3.1(T63)	0.46 ± 0.25	0.58 ± 0.30	2.46 ± 0.33	0.33 ± 0.18	3.82 ± 0.26	–
Commonwealth Scientific and Industrial Research Organisation Mark version 3.0 (CSIRO Mk3.0)	0.49 ± 0.22	0.36 ± 0.26	1.72 ± 0.23	0.29 ± 0.16	2.86 ± 0.22	3.14 ± 0.34
Goddard Institute for Space Studies Model E-R (GISS-ER)	–	0.31 ± 0.17	1.67 ± 0.26	0.40 ± 0.06	–	3.75 ± 0.27
MIROC3.2(medres)	−0.07 ± 0.24	1.73 ± 0.36	1.64 ± 0.25	0.33 ± 0.14	3.62 ± 0.26	4.02 ± 0.45
Meteorological Research Institute Coupled General Circulation Model, version 2.3.2a (MRI CGCM2.3.2)	0.79 ± 0.23	0.07 ± 0.31	1.31 ± 0.23	0.54 ± 0.25	2.71 ± 0.33	2.98 ± 0.48
HadGEM1	0.68 ± 0.20	0.01 ± 0.27	2.48 ± 0.23	−0.34 ± 0.13	2.82 ± 0.29	3.05 ± 0.52
HadSM3	0.23 ± 0.08	0.85 ± 0.18	2.36 ± 0.05	−0.34 ± 0.05	3.10 ± 0.18	–
HadSM3b	0.45 ± 0.10	0.58 ± 0.09	2.13 ± 0.06	−0.22 ± 0.07	2.93 ± 0.12	3.30 ± 0.17
Ensemble	0.51 ± 0.34	0.43 ± 0.56	1.91 ± 0.48	0.16 ± 0.32	3.18 ± 0.42	3.33 ± 0.47

changes in net surface LW to be dominated by changes in column-integrated water vapor, which increased with surface temperature. The SW surface feedback Y_{SW} is small and is the net effect of complicated, and uncertain, processes involving changes in clouds, water vapor, and surface albedo, all of which can change in response to ΔT and impact the surface SW radiation. For a stable system the surface must lose the excess heat gain; this is achieved by a large negative surface LH feedback, $Y_{LH} = -2.22 \pm 0.25$ W m^{-2} K^{-1} for the multimodel ensemble, which was also noted by GW08. Thus, as ΔT increases the surface evaporative cooling strongly increases. This interaction between net LW radiative heating and enhanced evaporative cooling provides an important ocean–atmosphere feedback (e.g., Ramanathan 1981).

b. Land–sea contrast

We now separate the global regressions into land and sea components. Figure 2a shows the time series of annual-mean land-mean, sea-mean, and global-mean ΔT in the Canadian Centre for Climate Modelling and Analysis (CCCma) Coupled General Circulation Model, version 3.1 (T47 resolution) [CGCM3.1(T47)] $2 \times CO_2$ experiment. It is clear that land temperatures increase more than sea temperatures (see Fig. 2a). This differential

TABLE 2. Components of the global-mean surface climate feedback parameter (W m^{-2} K^{-1}) for various slab-ocean GCMs forced by $2 \times CO_2$. Uncertainties are as in Table 1. Also shown for comparison is the net TOA feedback parameter (Y'_{Net}) determined by GW08.

	Y_{LW}	Y_{SW}	Y_{LH}	Y_{SH}	Y_{Net}	Y'_{Net} (GW08)
CCSM3.0	–	−0.03 ± 0.08	−2.23 ± 0.07	0.39 ± 0.04	–	−1.06 ± 0.10
CGCM3.1(T47)	0.82 ± 0.08	0.10 ± 0.08	−2.26 ± 0.09	0.31 ± 0.06	−1.03 ± 0.07	−1.26 ± 0.12
CGCM3.1(T63)	1.10 ± 0.09	−0.12 ± 0.10	−2.43 ± 0.11	0.31 ± 0.06	−1.14 ± 0.09	–
CSIRO Mk3.0	0.69 ± 0.09	0.36 ± 0.11	−2.30 ± 0.10	0.32 ± 0.07	−0.92 ± 0.09	−0.96 ± 0.14
GISS-ER	–	0.02 ± 0.08	−2.70 ± 0.13	0.32 ± 0.03	–	−1.40 ± 0.12
MIROC3.2(medres)	0.99 ± 0.07	0.06 ± 0.11	−2.18 ± 0.07	0.20 ± 0.04	−0.93 ± 0.08	−0.95 ± 0.13
MRI CGCM2.3.2	1.05 ± 0.09	−0.06 ± 0.12	−2.14 ± 0.09	0.26 ± 0.09	−0.89 ± 0.13	−0.93 ± 0.18
HadGEM1	0.91 ± 0.06	0.21 ± 0.08	−2.22 ± 0.07	0.43 ± 0.04	−0.67 ± 0.09	−0.63 ± 0.15
HadSM3	1.26 ± 0.03	−0.35 ± 0.06	−1.90 ± 0.02	0.06 ± 0.02	−0.92 ± 0.06	–
HadSM3b	1.26 ± 0.03	−0.31 ± 0.03	−1.82 ± 0.02	0.04 ± 0.03	−0.84 ± 0.04	−0.89 ± 0.06
Ensemble	1.01 ± 0.20	−0.01 ± 0.22	−2.22 ± 0.25	0.26 ± 0.13	−0.92 ± 0.14	−0.96 ± 0.26

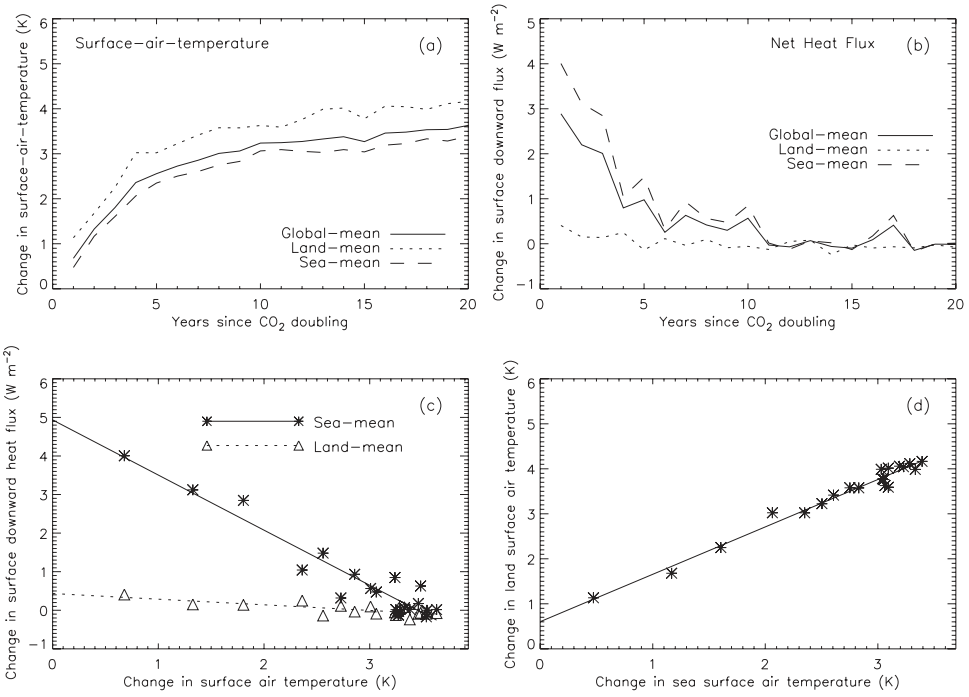

FIG. 2. Time series of the change in land-mean, sea-mean, and global-mean (a) surface air temperature and (b) net surface heat flux for CGCM3.1(T47) forced by $2 \times CO_2$. Also shown is (c) the land-mean and sea-mean regression of N against global-mean ΔT, and (d) the regression of land-mean surface air temperature change against sea-mean surface air temperature change.

warming is often referred to as the land–sea warming contrast and is not just a transient effect because it also occurs in equilibrium conditions (e.g., Sutton et al. 2007; Joshi et al. 2008). Figure 2b shows the time series of land-mean, sea-mean, and global-mean change in annual-mean net surface heat flux N. Over land N follows a different path to N over the sea (see Fig. 2b). Because of the land areas having a relatively small heat capacity, N reaches equilibrium ($N = 0$) quickly; in fact, the surface energy imbalance has almost been eliminated within the first year. Regressing land-mean N against ΔT, Fig. 2c, therefore, reveals little information because the land-mean N has already reached equilibrium. Furthermore, despite quickly reaching energy balance, land temperatures will eventually be dominated by the ocean response, which is slower to respond because of its larger heat capacity. Land areas are therefore not allowed to follow their own linear path as described by Eq. (1). We note however that global-mean values are dominated by the oceans, where we observe Eq. (1) to work well.

As part of the adjustment land temperatures warm and rapidly regain energy balance (see also Williams et al. 2008). We check the suggestion that land temperatures rapidly warm faster than ocean temperatures by regressing land-mean ΔT against sea-mean ΔT, Fig. 2d. The intercept of the regression line with the land-mean ΔT axis shows that in this model [CGCM3.1(T47)] the land warms on average by ~0.6 K before ocean temperatures respond. Because the rest of the points lie on a straight line this initial nonlinearity must have occurred within the first few months and thereafter a constant ''differential land/sea warming ratio'' (determined from the gradient of the regression line) is a good approximation. For this particular model, the differential land/sea warming ratio is 1.05 ± 0.04, which is barely distinct from unity, so both land and sea temperatures warm equally together after the initial land warming.

It is well known that reducing land evapotranspiration increases land temperatures (e.g., Shukla and Mintz 1982). Thus, if the rapid global decrease in the surface LH flux found in section 3a is accompanied by a similar reduction over land areas, this could result in land warming. In addition, increasing CO_2 concentration reduces the stomatal conductance of plants, which reduces the surface evapotranspiration flux to the atmosphere. Both Boucher et al. (2008) and Dong et al. (2009) showed that such an effect does contribute to the land–sea warming contrast under CO_2 forcing. However, a similar analysis of a solar forcing experiment (see section 4), in which the reductions in the surface LH flux are small compared to the CO_2 experiment, also reveals an initial land warming. We therefore suggest that the initial land

TABLE 3. Adjustment in land-mean temperatures, occurring before sea-mean temperature change, and the differential land/sea warming ratio for GCMs forced by $2 \times CO_2$. The adjustments and ratios are diagnosed from the land temperature intercept and gradient of the land-mean against sea-mean temperature change regression line. Uncertainties are as in Table 1.

	Land adjustment (K)	Differential land/sea warming ratio
CCSM3.0	0.59 ± 0.15	1.07 ± 0.07
CGCM3.1(T47)	0.60 ± 0.11	1.05 ± 0.04
CGCM3.1(T63)	0.53 ± 0.12	1.11 ± 0.04
CSIRO Mk3.0	0.49 ± 0.10	1.12 ± 0.04
GISS-ER	0.30 ± 0.27	1.30 ± 0.14
MIROC3.2(medres)	0.26 ± 0.13	1.30 ± 0.04
MRI CGCM2.3.2	0.20 ± 0.13	1.20 ± 0.06
HadGEM1	0.64 ± 0.17	1.24 ± 0.06
HadSM3	0.68 ± 0.06	1.47 ± 0.02
HadSM3b	0.64 ± 0.05	1.44 ± 0.02
Ensemble	0.49 ± 0.18	1.23 ± 0.15

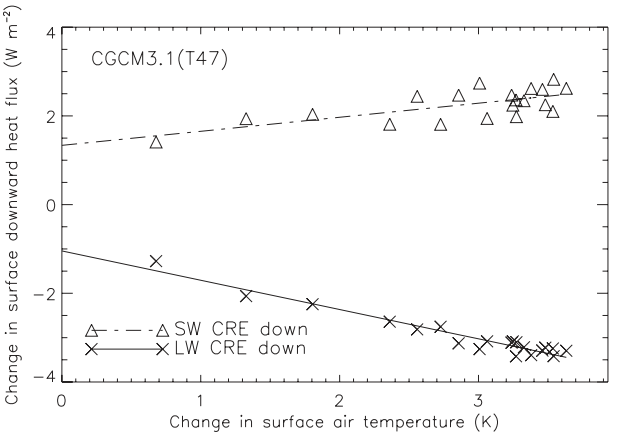

FIG. 3. Change in annual-mean global-mean downwelling LW and SW CRE as a function of annual-mean ΔT for CGCM3.1(T47) forced by $2 \times CO_2$. Fluxes are defined as positive downward. The lines are the regressions and the symbols are annual means.

warming cannot be solely explained by a forcing-dependent reduction of the LH flux over land. Instead, it may involve many complicated near-surface effects (e.g., see Dong et al. 2009; Joshi et al. 2008).

We analyze the other slab-ocean models in a similar way and report the results for the initial land warming and the differential land/sea warming ratio in Table 3. The initial land warming is a robust feature across models, with an ensemble mean of ~0.5 K (Table 3). The differential land/sea warming ratio evaluated here is smaller than the land/sea warming ratio that includes the initial land temperature adjustment (e.g., Sutton et al. 2007), but remains greater than unity in most models. Given that the ratio is greater than one there must be other processes that act on longer time scales that further enhance land temperatures compared to sea temperatures. These other processes must scale with global ocean temperature change so as to maintain a constant differential land/sea warming ratio. It is likely that these processes are near-surface effects, linked to the hydrological cycle and feedbacks that are different over the land and sea (see Joshi et al. 2008).

c. Clouds

Cloud behavior in response to climate forcing is regarded as one of the most uncertain aspects of a climate model, and perhaps of our understanding of the climate system as a whole (e.g., Randall et al. 2007; Stephens 2005). However, recent work (e.g., GW08; Andrews and Forster 2008; Williams et al. 2008) showed that some of the uncertainty normally associated with cloud feedback may have been misdirected. GW08 showed that clouds can quickly respond to CO_2 forcing, that is, as part of tropospheric adjustment, while Andrews and Forster (2008) showed that including this process as part of the forcing (rather than the feedback) reduces the range of model-predicted cloud feedback. On the other hand, because this rapid cloud adjustment varies between models, it increases our uncertainty in the forcing. Nevertheless, if cloud adjustment to CO_2 forcing is a real effect in climate models, then we should be able to observe this from the surface energy fluxes.

We investigate cloud adjustment by regressing the change in surface downwelling LW and SW cloud radiative effect (ΔCRE) components, determined as the difference between all and clear skies, against ΔT. Figure 3 shows such a regression for the CGCM3.1(T47) $2 \times CO_2$ experiment. The intercepts with the ΔCRE axis represent the surface cloud forcing components (FC_j), while the gradients of the regression lines represent the surface cloud feedback parameters (YC_j). Both downwelling $\downarrow$ LW and SW show significant nonzero surface cloud forcing components for this model (Fig. 3). In fact, $FC_{LW}\downarrow = -1.04 \pm 0.12$ and $FC_{SW}\downarrow = 1.34 \pm 0.23$, so cloud adjustment acts to decrease the amount of LW and increase the amount of SW radiation reaching the surface (see below for discussion on cloud-masking issues). This finding is consistent with the results of GW08 and Andrews and Forster (2008) who found that tropospheric adjustment to CO_2 forcing leads to reductions in cloud cover, which would decrease the LW radiation and increase the SW radiation reaching the surface. Because the climate evolves on longer time scales according to ΔT, the cloud feedback parameters indicate that the SW and LW downwelling CRE components increase and decrease, respectively, which may indicate further cloud cover reduction.

TABLE 4. Components of the downwelling global-mean $2 \times CO_2$ surface cloud forcing (W m^{-2}) and surface cloud feedback (W m^{-2} K^{-1}). All values are defined as positive down. Values are determined from the regressions of CRE against ΔT. Uncertainties are as Table 1.

	$FC_{LW}\downarrow$	$FC_{SW}\downarrow$
CGCM3.1(T47)	−1.04 ± 0.12	1.34 ± 0.23
CGCM3.1(T63)	−1.24 ± 0.13	1.72 ± 0.36
MIROC3.2(medres)	−0.84 ± 0.10	1.52 ± 0.38
MRI CGCM2.3.2	−0.78 ± 0.28	0.55 ± 0.34
HadGEM1	−0.47 ± 0.11	0.67 ± 0.27
HadSM3	−0.63 ± 0.03	1.19 ± 0.19
Ensemble	−0.83 ± 0.28	1.14 ± 0.43
	$YC_{LW}\downarrow$	$YC_{SW}\downarrow$
CGCM3.1(T47)	−0.66 ± 0.04	0.32 ± 0.08
CGCM3.1(T63)	−0.65 ± 0.04	0.23 ± 0.12
MIROC3.2(medres)	−0.66 ± 0.03	0.52 ± 0.11
MRI CGCM2.3.2	−0.63 ± 0.11	0.02 ± 0.13
HadGEM1	−0.59 ± 0.03	0.40 ± 0.08
HadSM3	−0.52 ± 0.01	0.29 ± 0.06
Ensemble	−0.62 ± 0.05	0.30 ± 0.15

The other models can be analyzed in a similar way; Table 4 shows the $2 \times CO_2$ downwelling cloud forcing and feedback components. The qualitative behavior described above for CGCM3.1(T47) is robust across models, although the magnitude of the adjustment varies. Unfortunately, our cloud forcing components will be contaminated by cloud-masking effects, that is, without an instantaneous $2 \times CO_2$ surface CRE (resulting from cloud masking), we cannot separate an instantaneous cloud-masking effect from a cloud adjustment. Andrews and Forster (2008) found that the instantaneous TOA CRE is significant in the LW (~ -0.5 W m^{-2}), but negligible in the SW; we see no reason why this qualitative behavior should be different for the surface instantaneous CRE. Hence, we do not believe the large magnitude of the SW$\downarrow$ cloud forcing component, in particular (multimodel ensemble = 1.14 ± 0.43 W m^{-2}), to be the result of cloud masking. However, we further note that our reported surface cloud feedback components will also be affected by cloud-masking errors because changes in CRE do not necessarily imply a change in cloud properties (e.g., Soden et al. 2004, 2008). Therefore, we are not attempting to present a quantified estimate of surface cloud feedback, but we use these results as further evidence of rapid cloud adjustments to CO_2 forcing in climate models.

4. Solar forcing

We now investigate the dependence of these results on the forcing agent by comparing the $2 \times CO_2$ experiment results with a solar forcing experiment using HadSM3 in which the solar irradiance is instantaneously increased, as described in Gregory et al. (2004), and thereafter held constant.

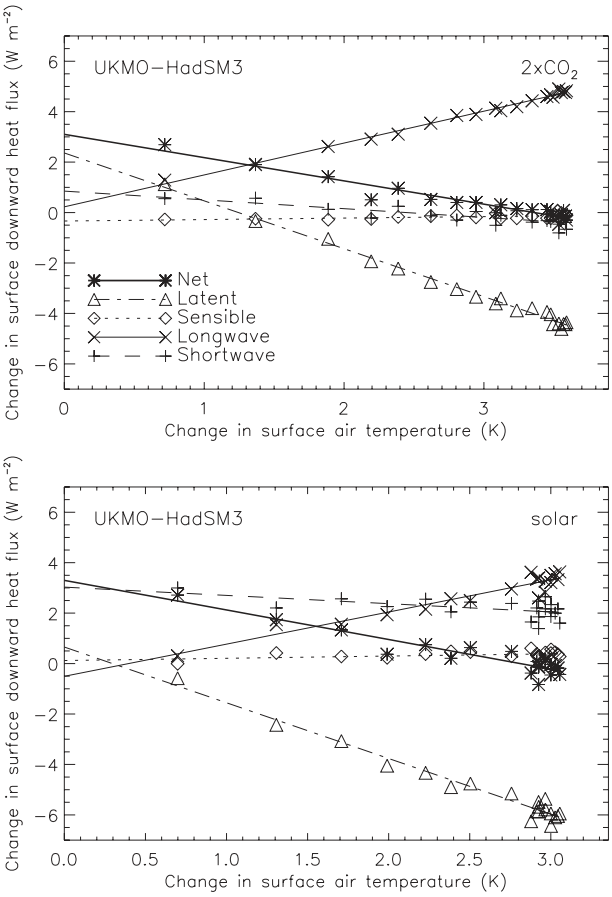

FIG. 4. Change in annual-mean global-mean surface heat fluxes N as a function of annual-mean ΔT for HadSM3 forced by (top) $2 \times CO_2$ and (bottom) a solar increase. All heat fluxes are defined as positive downward. The lines are the regressions and the symbols are annual means.

Figure 4 shows the surface heat flux regressions for an instantaneous $2 \times CO_2$ and solar increase experiment using the same model (HadSM3). As with the CO_2 experiment, the solar experiment demonstrates linear behavior, suggesting that the surface forcing response framework [Eq. (1)] may not only be a robust feature across models forced by CO_2 changes, but also across different forcing agents. A comparison of the diagnosed surface forcing and feedback components is shown in Fig. 5. The net surface forcing in both experiments are of similar sizes, and thus aid a direct comparison between the experiments without the need to normalize by the magnitude of the forcing. The significant difference between the solar and CO_2 surface forcing is that the solar forcing is predominantly composed of the SW radiation component, supporting the idea that solar forcings

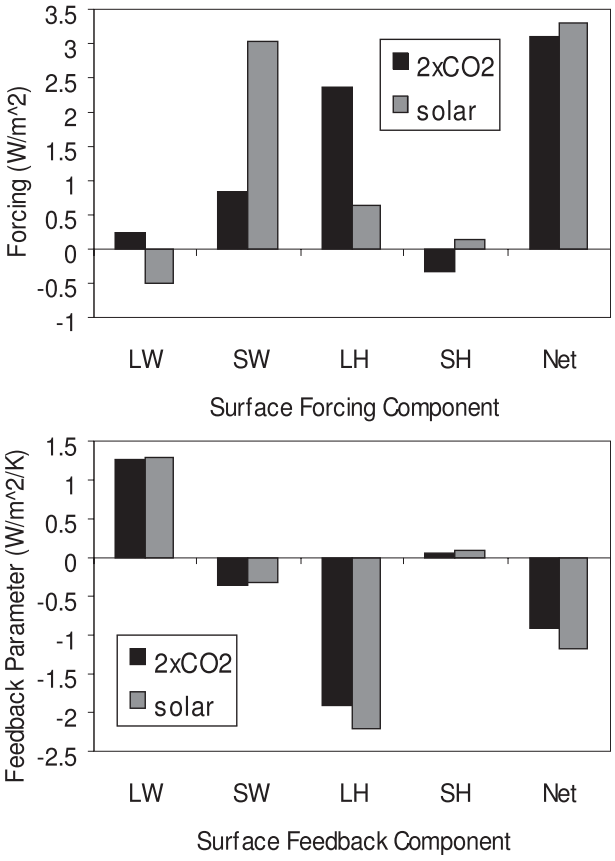

FIG. 5. Comparison of the adjusted surface forcing and feedback components, as diagnosed from the N intercepts and gradients of the regression lines of Fig. 4, for the HadSM3 $2 \times CO_2$ and solar increase experiment. The solar surface forcing is predominantly radiative (i.e., SW) while the CO_2 surface forcing is predominantly composed of an induced LH reduction.

are predominantly absorbed by the surface, and so more energy is available to enhance evaporation, given sufficient soil moisture over land. In comparison, the CO_2 surface radiative forcing is smaller and the net forcing is predominantly the result of an induced turbulent flux component (the implications of this for the hydrological cycle are discussed in section 5).

The utility of using a forcing definition that includes both stratospheric and tropospheric adjustment is that it leads to a climate feedback parameter that is less dependent on the forcing agent compared to conventional definitions (e.g., Shine et al. 2003; Hansen et al. 2005). Figure 5 suggests that the surface climate feedback components are similar. In fact, the components are statistically indistinguishable between the two experiments, except for the LH component, which leads to a small difference in the net feedback parameter. We note that the LH flux in the solar experiment has been determined from the upward moisture flux using the LH of

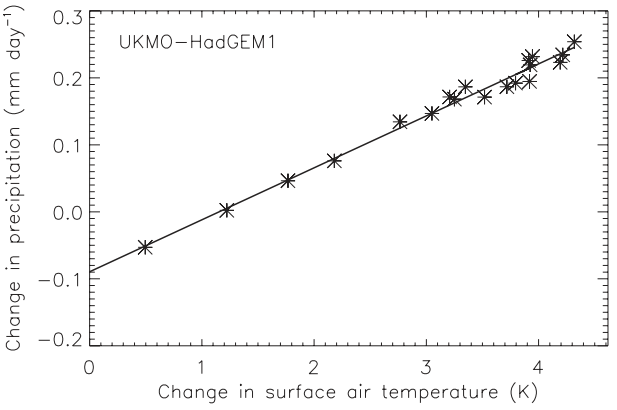

FIG. 6. Change in annual-mean global-mean precipitation rate (mm day^{-1}) as a function of annual-mean ΔT for HadGEM1 forced by $2 \times CO_2$. The line is the regression and the symbols are annual means.

condensation in this model. While this is not entirely accurate, because a small part of the moisture flux will come from sublimation, we find that the LH flux is determined accurately enough to have no impact on our conclusions. The root cause of this difference in the LH surface feedback component remains unclear, but we note that despite the difference being small it, may be worth further investigation.

5. Implications for the hydrological cycle

We now focus on what we can learn from the surface forcing response framework about the influence of forcing mechanisms on the earth's hydrological cycle.

a. Precipitation adjustment to CO_2 forcing

We noted in sections 3 and 4 that a robust feature across models in response to $2 \times CO_2$ is a rapid reduction in the LH flux to the atmosphere. Given that the LH flux controls the transportation of moisture from the surface to the atmosphere, this may have significant implications for the earth's hydrological cycle. Figure 6 shows the regression of the change in the annual-mean global-mean precipitation rate ΔP against annual-mean global-mean ΔT for the first 20 yr after CO_2 was doubled in the Hadley Centre Global Environmental Model version 1 (HadGEM1). The intercept of the ΔP axis indicates a rapid reduction in global-mean precipitation rate by $\sim$0.09 mm day^{-1} (or $\sim$2.9%) in this model. Similar regressions for other models (plots not shown) show this to be a robust feature, indicated by Table 5, which shows the intercepts of the ΔP axis (the fast response) and the gradients of the regression lines (the slow response scaling with ΔT). The initial reduction in precipitation rate is common betwen all of the models; the multimodel ensemble

TABLE 5. Adjustment to the global-mean precipitation rate as a fast response to $2 \times CO_2$ (not to ΔT) and the slow response (scaling with ΔT, referred to as the differential hydrological sensitivity) for slab-ocean GCMs. The adjustment is the result of conserving the tropospheric heat budget. The values in parentheses represent percentage changes. Uncertainties are as in Table 1.

	Precipitation adjustment [mm day^{-1} (%)]	Precipitation slow response [mm day^{-1} K^{-1} (% K^{-1})]
CCSM3.0	−0.04 ± 0.01 (−1.55 ± 0.18)	0.08 (2.77 ± 0.08)
CGCM3.1(T47)	−0.08 ± 0.01 (−2.91 ± 0.38)	0.08 (2.90 ± 0.13)
CGCM3.1(T63)	−0.09 ± 0.01 (−3.18 ± 0.43)	0.09 (3.04 ± 0.15)
CSIRO Mk3.0	−0.06 ± 0.01 (−2.39 ± 0.33)	0.08 (3.04 ± 0.14)
GISS-ER	−0.06 ± 0.01 (−2.07 ± 0.34)	0.09 (3.19 ± 0.15)
MIROC3.2(medres)	−0.06 ± 0.01 (−2.20 ± 0.31)	0.08 (2.75 ± 0.09)
MRI CGCM2.3.2	−0.05 ± 0.01 (−1.86 ± 0.31)	0.07 (2.86 ± 0.12)
HadGEM1	−0.09 ± 0.01 (−2.88 ± 0.27)	0.08 (2.50 ± 0.08)
HadSM3	−0.09 ± 0.01 (−2.98 ± 0.16)	0.07 (2.32 ± 0.05)
HadSM3b	−0.08 ± 0.01 (−2.69 ± 0.14)	0.06 (2.22 ± 0.05)
Ensemble	−0.07 ± 0.02 (−2.47 ± 0.54)	0.08 ± 0.01 (2.76 ± 0.32)

equals -0.07 ± 0.02 mm day^{-1} ($-2.47 \pm 0.54\%$). These results are consistent with previous modeling studies (e.g., Mitchell 1983; Yang et al. 2003) that prescribed sea surface temperatures (SST) in a $2 \times CO_2$ experiment and found similar reductions in the surface LH flux and precipitation rate; these results are analogous to our fast responses, although they differ in how they impose $\Delta T = 0$ (see discussion).

The subsequent response in precipitation rate to increases in ΔT ($\sim$0.08 mm day^{-1} K^{-1}, or $2.76 \pm 0.32\%$ K^{-1} for the multimodel ensemble), which we refer to as the "differential hydrological sensitivity" (see section 5b), is consistent with the increasing surface LH flux and an intensification of the hydrological cycle. Lambert and Webb (2008) also investigated the dependence of global-mean P on ΔT in contemporary GCMs, all models in our analysis fall within their 1.4–3.4 % K^{-1} range (see Table 5).

The initial reduction in the precipitation rate in response to increased CO_2 concentration can be explained on the grounds of the tropospheric heat budget (e.g., Mitchell 1983; Mitchell et al. 1987; Allen and Ingram 2002; Lambert et al. 2004; Lambert and Faull 2007). The tropospheric heating imbalance could be eliminated by the troposphere rapidly warming to reach a new radiative equilibrium, in an analogous way to that of the stratospheric response. It appears, however, that the most efficient way for the troposphere to regain its equilibrium is by finding a new radiative–convective equilibrium, which is largely achieved by reducing tropospheric condensational heating, which reduces precipitation rate, and is balanced by a reduced surface LH flux.

b. *Dependence of the hydrological sensitivity on forcing*

It is commonly reported that the earth's hydrological cycle is more sensitive to changes in solar radiation than changes in CO_2 concentrations (e.g., Allen and Ingram 2002; Gillett et al. 2004; Lambert et al. 2004). This is often quantified by showing that the hydrological sensitivity (defined as the percentage change in precipitation rate per ΔT, determined from equilibrium) is larger for a solar forcing (or similarly any scattering SW forcing) experiment than a CO_2 forcing [or, similarly, any greenhouse gas (GHG)] experiment (e.g., Feichter et al. 2004; Bala et al. 2008). We investigate reasons for this below.

Figure 7 shows the regression of the change in annual-mean global-mean precipitation rate ΔP against annual-mean global-mean ΔT for the HadSM3 $2 \times CO_2$ and solar experiment. From the ΔP intercept it is clear that the initial adjustment in the precipitation rate is much smaller for the solar forcing experiment than for the CO_2 case, with a reduction of $0.84 \pm 0.32\%$ and $2.98 \pm 0.16\%$, respectively (Table 6), and is consistent with the smaller adjustment in the surface LH flux (Fig. 5).

Through analysis of the final steady state alone we determine a hydrological sensitivity of $\sim$1.5% K^{-1} and $\sim$2.4% K^{-1} for the HadSM3 $2 \times CO_2$ and solar experiments, respectively. Hence, we recover the results of previous studies (e.g., Allen and Ingram 2002; Gillett et al. 2004; Lambert et al. 2004; Feichter et al. 2004; Bala et al. 2008) in which the hydrological cycle is more sensitive to solar forcing than CO_2. [In fact, these numbers are almost identical to those determined by Bala et al. (2008) using version 3 of the Community Climate Model (CCM3), which was forced by changes in CO_2 concentration and solar irradiance.] However, if we now remove the differences in the ΔT-independent initial adjustment to the precipitation rate, we determine the differential hydrological sensitivities (diagnosed from the gradient of the regression lines, Fig. 7) to be $2.32 \pm 0.05\%$ K^{-1} and $2.7 \pm 0.12\%$ K^{-1} for the $2 \times CO_2$ and solar experiment, respectively (Table 6).

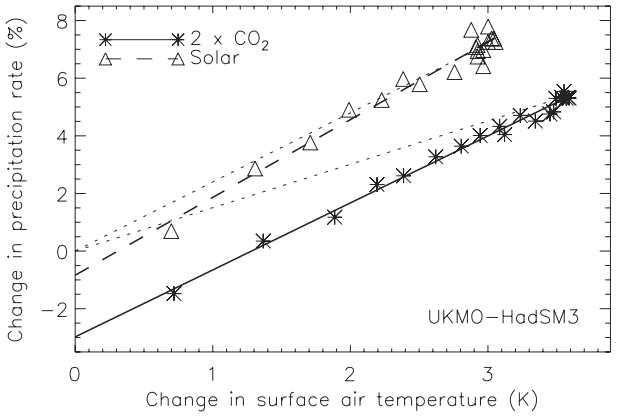

FIG. 7. Change in annual-mean global-mean precipitation rate (%) as a function of annual-mean ΔT for the HadSM3 2 × CO_2 and solar increase experiment. The precipitation adjustment before ΔT is larger for the CO_2 experiment, but as ΔT increases the precipitation response is more similar between the two forcing agents, indicated by the slope of the regression lines. Standard methods that compare the initial and final steady states are equivalent to diagnosing the gradient of the dotted lines.

This is a significantly reduced difference between the two hydrological sensitivities, with the remaining difference most probably being the result of the small difference in the surface LH feedback component found in section 4.

The limitation of diagnosing the hydrological sensitivity from standard methods that consider equilibrium states only is illustrated in Fig. 7. The dotted lines are constrained by the origin and the final steady states only, with their gradients being equivalent to the diagnosis the hydrological sensitivity via standard methods. While the transient and equilibrium methods result in only a small difference for the solar experiment, the standard method substantially underestimates the dependence of precipitation on ΔT for the CO_2 experiment because it does not take into account the fast response.

We conclude therefore that the difference in hydrological sensitivities between these two forcing agents is, in fact, predominantly due to a difference in an initial fast response in precipitation rate that occurs as a direct response to the forcing agent (not to ΔT), and subsequently as global temperatures increase the response of the global hydrological cycle is more similar between the two forcing mechanisms. It is also worth noting that while we have chosen a surface energy perspective as our starting point, one could equally infer this result from considering the time dependence of the tropospheric energy budget (e.g., Lambert and Faull 2007) because global-mean precipitation is controlled by the global-mean energy budget of the troposphere (Allen and Ingram 2002).

TABLE 6. The precipitation adjustment to the forcing agent and the differential hydrological sensitivity for the HadSM3 2 × CO_2 and solar increase experiment. Also shown for comparison is the hydrological sensitivity, defined as the equilibrium precipitation response divided by equilibrium ΔT (hydrological sensitivities diagnosed this way do not distinguish the initial adjustment before ΔT; see dotted lines on Fig. 7).

	2 × CO_2	Solar
Precipitation adjustment (%)	−2.98 ± 0.16	−0.84 ± 0.32
Differential hydrological sensitivity (% K^{-1})	2.32 ± 0.05	2.70 ± 0.12
Hydrological sensitivity (% K^{-1})	1.5	2.4

6. Discussion

Time-dependent analysis of surface heat fluxes forced by climate change mechanisms allows for the separation of surface forcing and climate response. This has given us a new perspective on climate change. Most notably it reevaluates the way the surface ''feels'' greenhouse forcing. The classical interpretation of the surface greenhouse forcing is purely radiative, that is, GHGs increase the downwelling LW radiation at the earth's surface. While this is important, our study has shown this to be only part of the story. GHGs also directly reduce the evaporative cooling of the earth's surface by reducing the surface LH flux. The way in which GHGs reduce the surface LH flux, and also precipitation rate, involve processes that act to restore the tropospheric heat budget. A simplified schematic is presented in Fig. 8.

The separation of rapid responses from longer-term responses reveals fundamental information about the hydrological cycle. We have shown that initially the precipitation rate depends directly on the forcing agent, and on longer time scales the precipitation response to ΔT (the differential hydrological sensitivity) is less sensitive to the forcing agent. However, note that in typical transient integrations, such as annually increasing CO_2 concentrations, the final forcing from the fast response would be realized after a number of years, so forcing and response would evolve together. The realized hydrological sensitivity would lie in between the differential and equilibrium values.

Our results agree with previous studies (e.g., Allen and Ingram 2002; Held and Soden 2006; Lambert and Webb 2008) in which global precipitation does not scale with Clausius–Clapeyron expectations in GCMs. Several recent observational studies (e.g., Wentz et al. 2007; Yu and Weller 2007; Allan and Soden 2007) suggest that the response of evaporation and precipitation to global

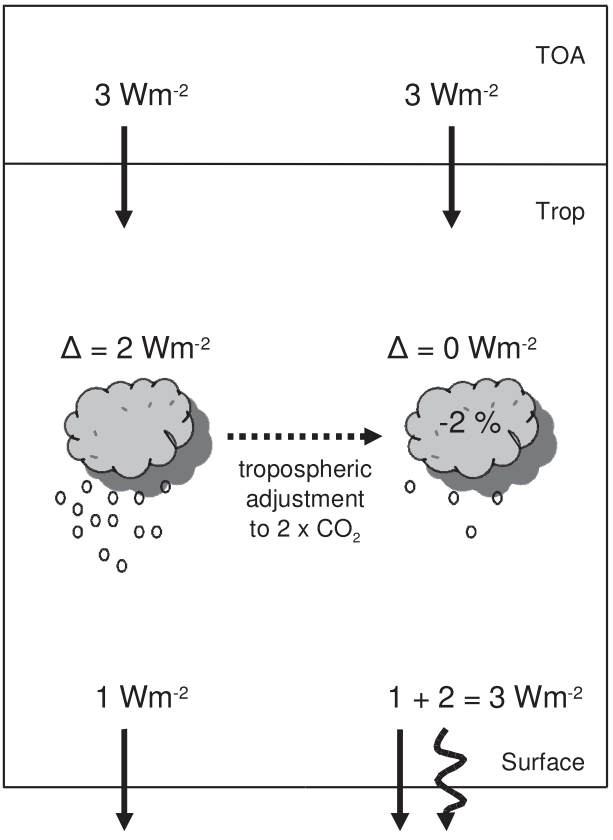

FIG. 8. Idealized schematic representing the global-mean surface LH flux and precipitation adjustment to $2 \times CO_2$ forcing. (left) $2 \times CO_2$ results in an adjusted tropopause *radiative* forcing of 3 W m^{-2}, but only 1 W m^{-2} at the surface, leading to a tropospheric heating imbalance of 2 W m^{-2}. (right) The tropospheric heat budget is conserved by reducing its condensational heating, which reduces precipitation rate by ~2%, and is balanced by a reduced surface LH flux to the troposphere (of ~2 W m^{-2}). Straight arrows represent radiative components, the curly arrow represents the LH flux, and Δ is the tropospheric heating imbalance.

warming is underestimated by models. In light of the fast and forcing-dependent response, we suggest careful consideration should be made to understand the forcing mechanisms that are changing during the observed time period and how these may contaminate the relationship between observed precipitation–evaporation changes and changes in global temperature, as well as accounting for natural climate variability (e.g., Lambert et al. 2008; Previdi and Liepert 2008).

The different response in precipitation rate for CO_2 and solar forcing experiments has increasingly been noted in geoengineering climate model experiments whereby the ΔT resulting from increased GHGs has been offset by reductions in solar irradiance (e.g., Bala et al. 2008; Lunt et al. 2008). In similar experiments, where, for example, CO_2 levels are instantaneously doubled at the same time as the solar irradiance is reduced, it would be interesting to see the time dependence of the change in precipitation rate; one might expect to see an initial rapid reduction (in response to the CO_2) and thereafter little changing. Geoengineering schemes should therefore consider the different time scales of the hydrological response for different forcing agents. In addition it would be beneficial if modeling groups performed additional fixed-SST experiments, because this would allow a straightforward way of analyzing the fast responses regionally (although the results may differ from the regression method; see the discussion below).

We distinguish between forcing, which includes fast responses, and climate response on the basis of time scale (e.g., see GW08); adjustments are evaluated before ΔT responds. We note two problems with this approach. First, this only requires global-mean ΔT to be zero, it sets no constraints on local temperatures; in fact, we have shown that land temperatures rapidly warm. This raises the question as to whether extrapolating ocean temperature change, rather than global-mean temperature change, to zero would be a better limit for analyzing the fast responses [see an analogous discussion between fixed-SST and fixed–surface temperature experiments (e.g., Shine et al. 2003; Hansen et al. 2005)]. But this too has deficiencies, for example, extrapolating to zero global SST change would still allow local SST changes that may result from a fast response of the upper ocean. One method might be to extrapolate all changes back to zero *local* temperature change. In principle, this should be possible, but in practice there is significant noise and so this approach would require a large ensemble. In our analysis we retain the global-mean $\Delta T = 0$ limit to be consistent with previous studies. Second, it is possible that fast responses could also change global-mean ΔT itself, but by construction we define global-mean ΔT to be zero, so we could not use this method to evaluate them. Nevertheless, we maintain that this method provides useful insights into climate change processes that analysis of steady states alone cannot determine.

7. Conclusions

We have developed a surface forcing response framework, governed by Eq. (1), that relates climate change to changes in the earth's surface energy budget. The framework allows for the separation of fast responses and slow climate feedbacks that scale with ΔT. The results show that the $2 \times CO_2$ adjusted surface *radiative* forcing is smaller than the TOA forcing, and so a surface latent heat forcing component and reduction in precipitation rate is induced to restore the tropospheric heat

budget (see Fig. 8). This fast response from the hydrological cycle is forcing dependent; for example, we found, in a solar increase experiment, that the surface forcing is predominantly radiative, and so a large adjustment to the hydrological cycle is not required. On longer time scales the climate evolves according to feedbacks associated with ΔT. These agree with earlier studies (e.g., Ramanathan 1981) and involve a positive net surface LW feedback and a strong negative latent heat feedback (net surface SW and the sensible heat flux change little with ΔT) and are found to be similar across different forcing agents. Analysis of the time-dependent surface energy balance over sea and land separately reveals that land areas rapidly regain energy balance, and significant land surface warming occurs before global sea temperatures respond.

The forcing-dependent adjustment to the hydrological cycle explains why previous studies have found differences in the hydrological sensitivity (defined as the percent change in precipitation rate per ΔT, determined from equilibrium) between CO_2 and solar forcing experiments. This difference is in fact predominantly due to a difference in an initial fast response in the precipitation rate, which is larger for CO_2 than solar forcings (see Fig. 7). The subsequent response of the global hydrological cycle to increases in global surface temperature is similar between the two forcing mechanisms.

To conclude, the TOA–tropopause radiative forcing concept helps us to understand the global temperature response to climate forcings; in this article, we have shown that using surface forcings gives additional insights, especially in understanding the response of the earth's hydrological cycle.

Acknowledgments. We acknowledge Gareth Jones for the solar experiment, the modeling groups, the Program for Climate Model Diagnosis and Intercomparison (PCMDI) and the WCRP's Working Group on Coupled Modelling (WGCM) for their roles in making available the WCRP CMIP3 multimodel dataset. Support of this dataset is provided by the Office of Science, U.S. Department of Energy. We also thank Isaac Held and two anonymous reviewers for useful comments. TA is funded by an NERC open CASE award with the Met Office. Work at the Hadley Centre was supported by the Integrated Climate Programme, GA01101 (Defra) and CBC/2B/0417_Annex C5 (MoD).

REFERENCES

Allan, R. P., 2006: Variability in clear-sky longwave radiative cooling of the atmosphere. *J. Geophys. Res.,* **111,** D22105, doi:10.1029/2006JD007304.

——, and B. J. Soden, 2007: Large discrepancy between observed and simulated precipitation trends in the ascending and descending branches of the tropical circulation. *Geophys. Res. Lett.,* **34,** L18705, doi:10.1029/2007GL031460.

Allen, M. R., and W. J. Ingram, 2002: Constraints on future changes in climate and the hydrological cycle. *Nature,* **419,** 224–232, doi:10.1038/nature01092.

Andrews, T., and P. M. Forster, 2008: CO_2 forcing induces semi-direct effects with consequences for climate feedback interpretations. *Geophys. Res. Lett.,* **35,** L04802, doi:10.1029/2007GL032273.

Bala, G., P. B. Duffy, and K. E. Taylor, 2008: Impact of geoengineering schemes on the global hydrological cycle. *Proc. Natl. Acad. Sci. USA,* **105,** 7664–7669, doi:10.1073/pnas.0711648105.

Boer, G. J., 1993: Climate change and the regulation of the surface moisture and energy budgets. *Climate Dyn.,* **8,** 225–239.

Boucher, O., G. Myhre, and A. Myhre, 2004: Direct human influence of irrigation on atmospheric water vapour and climate. *Climate Dyn.,* **22,** 597–603.

——, A. Jones, and R. A. Betts, 2008: Climate response to physiological forcing of carbon dioxide on plants in the Met Office Unified Model HadCM3. *Climate Dyn.,* **32,** 237–249, doi:10.1007/s00382-008-0459-6.

Collins, W. D., and Coauthors, 2006: Radiative forcing by well-mixed greenhouse gases: Estimates from climate models in the Intergovernmental Panel on Climate Change (IPCC) Fourth Assessment Report (AR4). *J. Geophys. Res.,* **111,** D14317, doi:10.1029/2005JD006713.

Davin, E. L., N. de Noblet-Ducoudré, and P. Friedlingstein, 2007: Impact of land cover change on surface climate: Relevance of the radiative forcing concept. *Geophys. Res. Lett.,* **34,** L13702, doi:10.1029/2007GL029678.

Dickinson, R. E., 1983: Land surface processes and climate-surface albedos and energy balance. *Adv. Geophys.,* **25,** 305–353.

Dong, B., J. M. Gregory, and R. T. Sutton, 2009: Understanding land–sea warming contrast in response to increasing greenhouse gases. Part I: Transient adjustment. *J. Climate,* in press.

Feichter, J., E. Roeckner, U. Lohmann, and B. Liepert, 2004: Nonlinear aspects of the climate response to greenhouse gas and aerosol forcing. *J. Climate,* **17,** 2384–2398.

Forster, P., and Coauthors, 2007: Changes in atmospheric constituents and in radiative forcing. *Climate Change 2007: The Physical Science Basis,* S. Solomon et al., Eds., Cambridge University Press, 129–234.

Gillett, N. P., A. J. Weaver, F. W. Zwiers, and M. F. Wehner, 2004: Detection of volcanic influence on global precipitation. *Geophys. Res. Lett.,* **31,** L12217, doi:10.1029/2004GL020044.

Gregory, J. M., and M. Webb, 2008: Tropospheric adjustment induces a cloud component in CO_2 forcing. *J. Climate,* **21,** 58–71.

——, and Coauthors, 2004: A new method for diagnosing radiative forcing and climate sensitivity. *Geophys. Res. Lett.,* **31,** L03205, doi:10.1029/2003GL018747.

Hansen, J., and Coauthors, 2005: Efficacy of climate forcings. *J. Geophys. Res.,* **110,** D18104, doi:10.1029/2005JD005776.

Held, I. M., and B. J. Soden, 2006: Robust responses of the hydrological cycle to global warming. *J. Climate,* **19,** 5686–5699.

Houghton, J. T., G. J. Jenkins, and J. J. Epharmus, Eds., 1990: *Scientific Assessment of Climate Change.* Cambridge University Press, 365 pp.

Joshi, M. M., J. M. Gregory, M. J. Webb, D. M. H. Sexton, and T. C. Johns, 2008: Mechanisms for the land/sea warming contrast exhibited by simulations of climate change. *Climate Dyn.,* **30,** 455–465, doi:10.1007/s00382-007-0306-1.

Lambert, F. H., and N. E. Faull, 2007: Tropospheric adjustment: The response of two general circulation models to a change

in insolation. *Geophys. Res. Lett.,* **34,** L03701, doi:10.1029/2006GL028124.

——, and M. J. Webb, 2008: Dependency of global mean precipitation on surface temperature. *Geophys. Res. Lett.,* **35,** L16706, doi:10.1029/2008GL034838.

——, P. A. Stott, M. R. Allen, and M. A. Palmer, 2004: Detection and attribution of changes in 20th century land precipitation. *Geophys. Res. Lett.,* **31,** L10203, doi:10.1029/2004GL019545.

——, A. R. Stine, N. Y. Krakauer, and J. C. H. Chiang, 2008: How much will precipitation increase with global warming? *Eos, Trans. Amer. Geophys. Union,* **89,** doi:10.1029/2008EO210001.

Liepert, B. G., J. Feichter, U. Lohmann, and E. Roeckner, 2004: Can aerosols spin down the water cycle in a warmer and moister world? *Geophys. Res. Lett.,* **31,** L06207, doi:10.1029/2003GL019060.

Lunt, D. J., A. Ridgwell, P. J. Valdes, and A. Seale, 2008: "Sunshade World": A fully coupled GCM evaluation of the climatic impacts of geoengineering. *Geophys. Res. Lett.,* **35,** L12710, doi:10.1029/2008GL033674.

Meehl, G. A., and Coauthors, 2007: Global climate projections. *Climate Change 2007: The Physical Science Basis,* S. Solomon et al., Eds., Cambridge University Press, 589–662.

Mitchell, J. F. B., 1983: The seasonal response of a general circulation model to changes in CO_2 and sea temperatures. *Quart. J. Roy. Meteor. Soc.,* **109,** 113–152.

——, C. A. Wilson, and W. M. Cunnington, 1987: On CO_2 climate sensitivity and model dependence of results. *Quart. J. Roy. Meteor. Soc.,* **113,** 293–322.

——, T. C. Johns, M. Eagles, W. J. Ingram, and R. A. Davis, 1999: Towards the construction of climate change scenarios. *Climatic Change,* **41,** 547–581.

National Research Council, 2005: *Radiative Forcing of Climate Change*. National Academies Press, 207 pp.

Pielke, R. A., Sr., 2001: Influence of the spatial distribution of vegetation and soils on the prediction of cumulus convective rainfall. *Rev. Geophys.,* **39,** 151–177.

Previdi, M., and B. G. Liepert, 2008: Interdecadal variability of rainfall on a warming planet. *Eos, Trans. Amer. Geophys. Union,* **89,** doi:10.1029/2008EO210002.

Ramanathan, V., 1981: The role of ocean-atmosphere interactions in the CO_2 climate problem. *J. Atmos. Sci.,* **38,** 918–930.

——, P. J. Crutzen, J. T. Kiehl, and D. Rosenfeld, 2001: Aerosols, climate, and the hydrological cycle. *Science,* **294,** 2119–2124, doi:10.1126/science.1064034.

Randall, D. A., and Coauthors, 2007: Climate models and their evaluation. *Climate Change 2007: The Physical Science Basis,* S. Solomon et al., Eds., Cambridge University Press, 589–662.

Shine, K. P., J. Cook, E. J. Highwood, and M. M. Joshi, 2003: An alternative to radiative forcing for estimating the relative importance of climate change mechanisms. *Geophys. Res. Lett.,* **30,** 2047, doi:10.1029/2003GL018141.

Shukla, J., and Y. Mintz, 1982: Influence of land-surface evapotranspiration of the earth's climate. *Science,* **215,** 1498–1501.

Soden, B. J., A. J. Broccoli, and R. S. Hemler, 2004: On the use of cloud forcing to estimate cloud feedback. *J. Climate,* **17,** 3661–3665.

——, I. M. Held, R. Colman, K. M. Shell, J. T. Kiehl, and C. A. Shields, 2008: Quantifying climate feedbacks using radiative kernels. *J. Climate,* **21,** 3504–3520.

Stephens, G. L., 2005: Cloud feedbacks in the climate system: A critical review. *J. Climate,* **18,** 237–273.

Sutton, R. T., B. Dong, and J. M. Gregory, 2007: Land/sea warming ratio in response to climate change: IPCC AR4 model results and comparison with observations. *Geophys. Res. Lett.,* **34,** L02701, doi:10.1029/2006GL028164.

Wentz, F. J., L. Ricciardulli, K. Hilburn, and C. Mears, 2007: How much more rain will global warming bring? *Science,* **317,** 233–235, doi:10.1126/science.1140746.

Wild, M., A. Ohmura, H. Gilgen, and D. Rosenfeld, 2004: On the consistency of trends in radiation and temperature records and implications for the global hydrological cycle. *Geophys. Res. Lett.,* **31,** L11201, doi:10.1029/2003GL019188.

Williams, K. D., W. J. Ingram, and J. M. Gregory, 2008: Time variation of effective climate sensitivity in GCMs. *J. Climate,* **21,** 5076–5090.

Yang, F., A. Kumar, M. E. Schlesinger, and W. Wang, 2003: Intensity of hydrological cycles in warmer climates. *J. Climate,* **16,** 2419–2423.

Yu, L., and R. A. Weller, 2007: Objectively analyzed air–sea heat fluxes for the global ice-free oceans (1981–2005). *Bull. Amer. Meteor. Soc.,* **88,** 527–539.